Oxidation reactions at variably sized transition metal centers: Fe_n^+ and $Nb_n^+ + O_2$ ($n = 1$–3)

S. K. Loh[a)]
Department of Chemistry, University of California, Berkeley, California 94720
Li Lian and P. B. Armentrout[b)]
Department of Chemistry, University of Utah, Salt Lake City, Utah 84112

(Received 11 May 1989; accepted 1 August 1989)

Cross sections for the reactions of Fe_n^+ and Nb_n^+ ($n = 1$–3) with O_2 are measured as a function of kinetic energy over a range of 0 to > 10 eV. In all systems, analysis yields insight into the kinetics and thermochemistry of the oxidation processes. Nb_n^+ reaction with O_2 exothermically near the Langevin–Gioumousis–Stevenson close-collision limit, driven by formation of strong NbO^+ and NbO bonds. Fe_n^+ are less reactive, although oxidation becomes progressively more facile as the size of the reactant increases from Fe^+ to Fe_3^+. In contrast to the Nb_n^+ systems, Fe_n^+ ($n = 2,3$) react at elevated energies by simple cluster fragmentation processes. Quantitative limits are established for ionic and neutral cluster oxide bond dissociation energies. Cross sections for formation of M_nO^+ from reaction of M_n^+ (Fe_3^+, Nb_2^+, and Nb_3^+) are observed to have both an exothermic and an endothermic feature. Since there is only one chemical pathway to form this product, it is suggested that there are activation barriers to formation of favorable reaction intermediates. A similar suggestion is required to explain product branching ratios involving metal dioxides which run counter to thermodynamic predictions.

I. INTRODUCTION

Transition metal surfaces and atoms have long been subjects of chemical scrutiny. Not surprisingly, investigations of these two regimes show substantial differences in both their physical and chemical properties, a reflection of the differences in both the electronic natures and the physical structures of atoms and surfaces. With recent experimental innovations,[1] the study of small clusters of transition metal atoms is now feasible and offers an exciting opportunity to explore the intermediate range of sizes.

A. Neutral clusters

Recently, experimental investigations have provided information on physical properties of transition metal clusters. Primary examples of such work have been photoionization studies of vanadium and niobium,[2(a)] nickel,[2(b)] copper,[2(c)] and iron,[2(d)] in which ionization thresholds have been measured or bracketed. Careful spectroscopic work has been performed primarily on metal dimers[3,4] yielding information on the bonding between metal atoms. The magnetic properties of bare and oxygenated iron clusters have also been investigated.[5]

By far, the most common way of studying the chemical properties of neutral clusters has been the use of flow tube techniques. In experiments of this type, a distribution of cluster sizes are created in a flow of He. Downstream, these species are exposed to a reagent at known concentrations. After some reaction time, all products are identified and measured, usually by photoionization followed by a time-of-flight analysis.

To date, iron clusters have been the most intensely studied, largely due to the efforts of Parks *et al.*,[6] Morse *et al.*,[7] and Whetten *et al.*[8] Reactions of Fe_n with molecular hydrogen have been carried out and have led to identification of a mechanism for dissociative chemisorption of H_2 on iron clusters. With long reaction times or high reagent concentrations, chemisorption reactions can be followed to completion. Such saturation experiments have been done on Fe_n using NH_3 and D_2O.[6] Average "saturation coverages" were found for each cluster. These show abrupt changes at certain cluster sizes, providing evidence for dramatic differences in geometries of clusters that differ by only one atom.

Flow tube techniques have also been applied to the reactivities of niobium clusters. The gross reaction patterns of D_2 and N_2 toward Nb_n have shown appreciable variation with cluster size.[7,9] Multicomponent rates for these reactions have been observed for certain niobium clusters, indicating that more than one structural isomer can be routinely formed.[10,11] Niobium clusters have been found to dehydrogenate benzene.[12,13] The extent of this reaction is sensitive to cluster size and source conditions. The postreaction ionization and fragmentation processes have been examined by St. Pierre *et al.*[14] These studies find that the internal energy of the cluster does influence the observed reactivity.

There have been only two studies of neutral transition metal cluster reactions with O_2 that we are aware of. Both involve oxidation of Fe_n in flow tube arrangements. Whetten *et al.* found that neutral iron clusters react to form Fe_nO_2 and Fe_nO.[8] At higher O_2 pressures, Fe_nO_{2m} was formed, although Fe_nO_{2m+1} were not observed at these O_2 pressures, indicating that molecular chemisorption dominates

[a)] Current address: IBM, Thomas J. Watson Research Center, Yorktown Heights, NY.
[b)] NSF Presidential Young Investigator, 1984–1989; Alfred P. Sloan Fellow; Camille and Henry Dreyfus Teacher-Scholar, 1988–1993.

 0021-9606/89/226148-16$02.10

the reactivity. In the absence of an energetic plasma, atomic Fe was found to be unreactive with O_2. This is reasonable since FeO formation is endothermic and FeO_2 production, although exothermic, requires three-body collisional stabilization. The second study, performed by Riley *et al.*, examined the oxidation of iron clusters from 1 to 60 atoms at relatively high O_2 pressures.[15] They found that Fe_n undergo extensive oxidation to form Fe_nO_m where n is slightly smaller than m for the larger clusters.

A great deal of information has been obtained through these studies making it clear that flow tube experiments present a powerful way of studying reactions of neutral clusters. However, a limitation of these studies is that it is difficult to observe a single specific reaction, or to unequivocally identify the reactants and their ensuing products. Moreover, reactions that involve cluster oxides and ionic clusters, which are also formed in these sources, can further confuse the issue. Ambiguities are also caused by product fragmentation during the ionization step prior to detection.

B. Ionic clusters

Studies of ionic clusters circumvent these problems. By using mass-spectrometric techniques, an ion of a single mass can be selected for study from the distribution of bare and partially oxygenated clusters that are emitted from a source. Furthermore, since the trajectories of ions can be controlled, cluster chemistry can be studied under relatively well-defined conditions. After reaction, ionic products can be unambiguously identified and easily detected.

The first studies of a bare transition metal cluster ion to take advantage of these properties were performed on Mn_2^+. Ion beam techniques were used to examine its bond dissociation energy (BDE)[16] and oxidation chemistry.[17] Recently, careful studies of the reactions of aluminum cluster ions with O_2[18,19] and D_2[20] have been performed. Collision-induced dissociation (CID) experiments have also provided information on the thermodynamic stabilities of clusters of main group metals[21] and transition metals, such as Fe_n^+ and Nb_n^+.[22–24]

The reactivities of transition metal cluster ions have also been examined in ion cyclotron resonance (ICR) experiments. Jacobson and Freiser have created mixed metal dimers within an ICR cell by forming a heteronuclear metal carbonyl complex followed by CID with an inert gas.[25,26] Smalley *et al.* have taken a different tack by injecting cluster ions created from a pulsed supersonic expansion into the ICR cell.[27] The chemisorption of H_2 on Nb_n^+ ($n = 7$–9) has been studied,[28] providing evidence that Nb_7^+ has a high reactivity compared to Nb_8^+ and Nb_9^+. $Nb_7O_2^+$ and $Nb_7H_2O_2^+$ were found to be considerably less reactive than the unoxidized cluster, an indication that the oxygen ligand can substantially influence the reactivities of metal clusters.

Flow tube experiments on ionic clusters have also been performed, allowing comparison to the analogous reactions of neutral clusters. In these, Fe_n and Fe_n^+ ($n < 23$) generally have decidedly different reactivities with H_2,[7,29] while different charge states of larger clusters generally show similar reactivities. Unlike the iron clusters, Nb_n, Nb_n^+, and Nb_n^- have reactivities that show identical qualitative dependences on cluster size.[12]

In this paper, the reactions of Fe_n^+ and Nb_n^+ ($n = 1$–3) with O_2 are studied by ion beam techniques. Reaction cross sections, measured as a function of kinetic energy, are presented. The energy thresholds allow determination of quantitative reaction thermochemistry of both ionic and neutral oxide species. The relative cross section behaviors are used to understand the general reactivities of each metal.

II. EXPERIMENTAL SECTION

Experiments were performed with a recently constructed guided ion beam apparatus. This instrument is designed to generate intense continuous beams of mass-selected, thermalized cluster ions. Cluster reactions can be examined over collision energies that range from near thermal energies to hundreds of eV. Interaction of the ionic metal species with molecular oxygen occurs at low pressures and at well-defined kinetic energies. Since a complete description of the design and operation of the instrument has been given in a recent publication,[23] only a brief description is presented here.

A copper vapor laser (with a 7 kHz repetition rate and ~25 W average power) ablates a 6.4 mm diam sample rod. The iron or niobium rod rotates and translates to continuously expose fresh metal to the tightly focused laser. Ions of either metal are created directly from the laser vaporization process; therefore, an external ionizer is neither required nor used.[30] To entrain the metal vapor, the high vaporization rate demands a continuous flow of the helium carrier gas, here 6000 sccm. Within the 5.7 cm long, 2 mm diam. clustering nozzle, a typical cluster should undergo $> 10^5$ collisions, dissipating excess internal energy that may reside in the cluster from the vaporization process.[30]

The resulting distribution of clusters and atoms undergoes a mild supersonic expansion cooling internal and translational degrees of freedom further.[31] The ions are subsequently gently focused through three differentially pumped regions and then accelerated into a 60° sector magnet. The momentum analyzer (1–1000 amu) has sufficient resolving power to cleanly select ions of a single mass. This mass-selected ion beam is decelerated to a well-defined kinetic energy and then injected into an octopole ion beam guide.[32] The octopole passes through a reaction cell in which the metal ions interact with O_2. To minimize multiple collision events, the O_2 pressure is kept at ~0.1 mTorr.[33] The octopole consists of eight parallel cylindrical rods arranged with radial symmetry. Opposite phases of rf voltage are applied to alternate rods, creating a radial potential well. Within the ion guide, the motion of the ions in the axial direction is unperturbed, but scattered ions with transverse motion (that would otherwise be lost) are effectively trapped. Consequently, efficient product ion collection is maximized. After reaction, the transmitted ion beam and product ions drift from the octopole and are mass analyzed by a quadrupole mass filter (5–1000 amu). Ion intensities are measured with standard pulse counting techniques.

III. DATA ANALYSIS

A complete experiment consists of measuring the intensities of all product ions as functions of the interaction energy. These intensities are converted to a total cross section via Eq. (1)

$$I_r = (I_r + \Sigma I_p)\exp(-\sigma_{\rm tot} n_D l)\,, \quad (1)$$

$$\sigma_p(E) = \sigma_{\rm tot}(I_p/\Sigma I_p) \quad (2)$$

as outlined previously.[32] The subscripts r and p refer to the transmitted reactant and the pth product ion, n_D is the reactant gas number density, and l is the effective path length (8.26 cm). Individual product cross sections are calculated with Eq. (2).

Cross section magnitudes have uncertainties of $\pm$ 20%, mainly due to the gas cell length and pressure measurement. Relative cross section magnitudes have uncertainties of 5%, assuming product collection is efficient, which has previously been shown to be good for most CID processes of iron and niobium cluster ions.[23,24,34] Low mass product ions may be less efficiently detected, because these ions can be formed with high transverse and low axial kinetic energies. This effect is most obvious at laboratory collision energies greater than the d.c. bias of the quadrupole (90 V) used here.

The distribution of ion energies is determined by using the octopole ion guide as a retarding energy analyzer. The octopole is particularly useful as an energy analyzer for two reasons. Low energy ion losses due to space charge effects are minimized and the uncertainties associated with contact potentials are eliminated because the retarding region is physically the same as the interaction region. The laboratory collision energies of an ion (of mass m) and a neutral reactant (of mass M) are converted to the center-of-mass (c.m.) frame by the equation $E(\text{c.m.}) = E(\text{lab})\cdot M/(m+M)$. The absolute uncertainty in the energy measurement is $\pm$ 0.05 eV lab.

Thermodynamic information is obtained from these studies by measuring the kinetic energy threshold of endothermic reactions and assuming that such reactions have no activation barriers in excess of the endothermicity. This assumption has proven to be generally valid for ion–molecule reactions where there are no restrictions due to spin or orbit constraints.[35] The possibility of barriers of this nature has been previously discussed for the reaction of Fe^+ and O_2 and experimentally determined to be absent.[36] For larger species, such as dimer or trimer ions, barriers cannot be determined *a priori*, because the structures and electron configurations for the cluster states are not known. However, we note that at long range, all of the potential surfaces are attractive because of the ion-induced dipole potential. Since a dimer or trimer ion will have considerably higher densities of low-lying electronic states than an atomic ion,[37,38] even more extensive mixing of the surfaces should occur. We anticipate that this mixing will result in avoided surface crossings, such that ground-state reactants correlate adiabatically to ground-state products without activation barriers. Thus we assume that the observed thresholds correspond to reaction endothermicities.

To obtain the threshold (E_0) of an endothermic process, we use the empirical model shown in Eq. (3)

$$\sigma_p(E) = \sigma_0(E - E_0)^N/E\,, \quad (3)$$

where E and E_0 are the c.m. collision and threshold energies. σ_0 is a scaling factor and N is an adjustable parameter. Before comparison to the data, Eq. (3) is convoluted over the distributions of ion energy and thermal motion of O_2.[35] Then the parameters N and E_0 are optimized to give the best nonlinear least-squares fit to the data. Past work has shown that Eq. (3) describes the theshold behaviors of numerous endothermic ion–molecule reaction cross sections and provides accurate reaction thermochemistry.[35]

IV. RESULTS AND DISCUSSION

The cross sections for reactions of Fe_n^+ and Nb_n^+ (n = 1–3) with O_2 are presented in the following sections. The reactions of iron are presented first. For each metal, the reaction of the atomic ion will be discussed first and the trimer ion reaction last. The cross section threshold behaviors will be discussed in regard to reaction thermochemistry and products formed. From the branching ratios and other features in the cross sections, mechanistic information will also be obtained and then discussed. As will be seen in all systems studied here, the product ions are invariably metal containing species, due to the relatively high ionization potentials (IPs) of O_2 and O. These values and other previously determined thermochemical data of interest are summarized in Table I. Also, the adduct M_n^+–O_2 is never observed,

TABLE I. Known thermochemical data (eV).[a]

	Fe		Nb	
	D^0_{298}	IP	D^0_{298}	IP
M	···	7.90 (0.001)[b]	···	6.88 (0.0003)[c]
M_2^+	2.72 (0.07)[d]	···	6.15 (0.15)[e]	···
M_2	1.12 (0.09)[d]	6.30 (0.01)[f]	5.19 (0.28)[e]	5.92 (0.32)[e]
M_2^+–M	1.64 (0.15)[g]	···	4.60 (0.15)[e]	···
M_2–M	1.79 (0.17)[g]	6.45 (0.05)[f]	4.3 (0.7)[e]	5.6 (0.8)[e]
M^+–O	3.57 (0.06)[h]	···	7.09(0.23)[i]	···
MO	4.23 (0.08)[j]	8.71 (0.10)[k]	8.12 (0.23)[e]	7.91 (0.02)[l]
M–O_2	3.60 (0.10)[m]	9.5 (0.5)[k]	9.67 (0.23)[e]	9.0 (0.5)[n]
M^+–O_2	2.0 (0.5)[o]		7.55 (0.55)[o]	
O_2	5.17 (0.001)[c]	12.07[c]		
O	···	13.62[c]		

[a] Uncertainties given in parentheses.
[b] J. Sugar and C. Corliss, J. Phys. Chem. Ref. Data **14**, Suppl. 2 (1985).
[c] M. W. Chase, C. A. Davies, J. R. Downey, D. J. Frurip, R. A. McDonald, and A. N. Syverud, J. Phys. Chem. Ref. Data **14**, Suppl. 1 (1985) (JANAF Tables).
[d] Reference 34.
[e] Reference 24.
[f] Reference 2(d).
[g] Reference 23.
[h] Reference 36.
[i] From $D^0(Nb^+\text{–}O) = D^0(NbO) + IP(Nb) - IP(NbO)$.
[j] Summarized in Ref. 36.
[k] Reference 45.
[l] J. M. Dyke, A. M. Ellis, M. Feher, A. Morris, A. J. Paul, and J. C. H. Stevens, J. Chem. Soc. Faraday Trans. 2 **83**, 1555 (1987).
[m] S. Smoes and J. Drowart, High Temp. Sci. **17**, 31 (1984).
[n] G. Balducci, G. Gigli, and M. Guido, J. Chem. Phys. **85**, 5955 (1986).
[o] Calculated from $D^0(M^+\text{–}O_2) = D^0(MO_2) + IP(M) - IP(MO_2)$.

since this species always has enough energy to dissociate back to reactants or to form products of exothermic reactions.

It will be seen that the energy-dependent reaction cross sections for individual products can have very complicated behavior. Previous experience has demonstrated to us that increases in individual product cross sections can generally be associated with the opening of a new reaction channel for that particular product, and that decreases in cross sections are usually associated with the onset of a dissociative process and sometimes a competing channel. While more subtle dynamic effects can also contribute to changes in cross section behavior, it seems reasonable to identify cross section features with specific reaction channels when a one-to-one correspondence can be made between the experimentally observed onset of the feature and the calculated thermodynamics of the channel. Further, when the decrease in one product cross section can be correlated with the increase in another, it seems reasonable to attribute the increasing cross section to a specific dissociation pathway.

Exothermic cross sections are compared to the Langevin–Gioumousis–Stevenson (LGS) model for barrierless ion–molecule reactions[39] given by Eq. (4)

$$\sigma_{\mathrm{LGS}}(E) = \pi e(2\alpha/E)^{1/2}, \tag{4}$$

where α is the polarizability of the neutral molecule, e is the fundamental charge, and E is the center-of-mass (c.m.) collision energy. Since this model merely predicts a cross section for close collisions, it represents an upper limit to the *reaction* cross section. At higher energies, the collision cross section is no longer adequately described by Eq. (4), but is more closely related to a simple hard-sphere cross section.

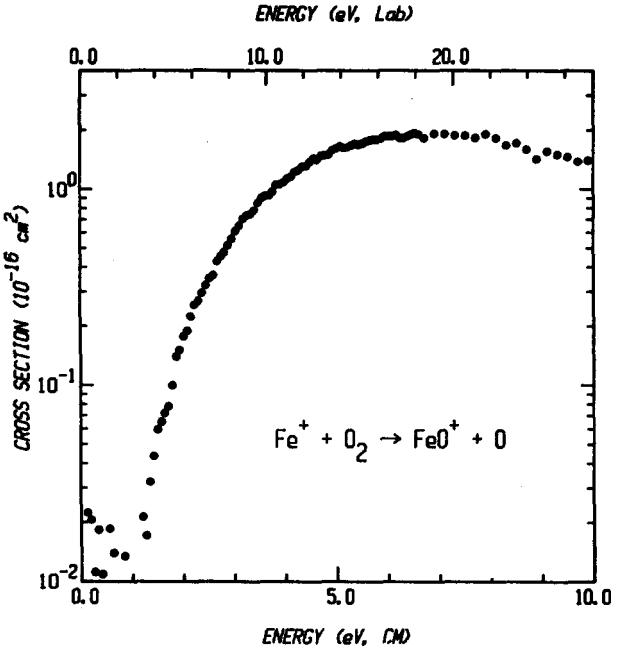

FIG. 1. The oxidation reaction of the atomic iron ion $Fe^+ + O_2 \rightarrow FeO^+ + O$. The reaction cross section is plotted as functions of collison energy in the center-of-mass (lower x axis) and laboratory (upper x axis) frames.

A. Iron oxidation reactions

1. $Fe^+ + O_2$

Formation of FeO^+ is the only possible iron-containing ionic product (excluding the adduct) in the reaction of Fe^+ with oxygen

$$M^+ + O_2 \rightarrow MO^+ + O, \tag{5}$$

where M = Fe. This reaction has been discussed in detail in a recent publication.[36] The cross section for reaction of ground-state $Fe^+(^6D)$ created by the laser vaporization source is reproduced in Fig. 1 for completeness and for comparison with the systems which follow. The FeO^+ cross section rises from a threshold of ~ 1.6 eV to a maximum of ~ 2 Å^2. The sharp rise in the cross section slows near the bond dissociation energy (BDE) of O_2, which is 5.2 eV. This is expected since the FeO^+ product can begin to decompose to $Fe^+ + O$ at this energy. Analyses of this system and the reaction of Fe^+ with ethylene oxide have yielded the BDE $D^0_{298}(Fe^+\text{–}O) = 3.57 \pm 0.06$ eV.[36]

2. $Fe_2^+ + O_2$: Reaction products and thermochemistry

The cross sections of the iron dimer ion reactions with O_2 are shown in Fig. 2. The complexity, relative to the atomic system, is immediately evident. The reactions which are possible in this system are listed in Table II along with the associated thermochemistry calculated from Table I. All four possible ionic reaction products are observed. The total cross section (σ_{tot}) varies smoothly with energy, belying the complex reactivity that lies below. At low energies, the energy dependence of σ_{tot} reflects the exothermic behavior of the Fe^+ product channel, i.e., it increases with decreasing collision energies as predicted by the LGS model, although its magnitude is smaller than σ_{LGS} by about a factor of 4. At

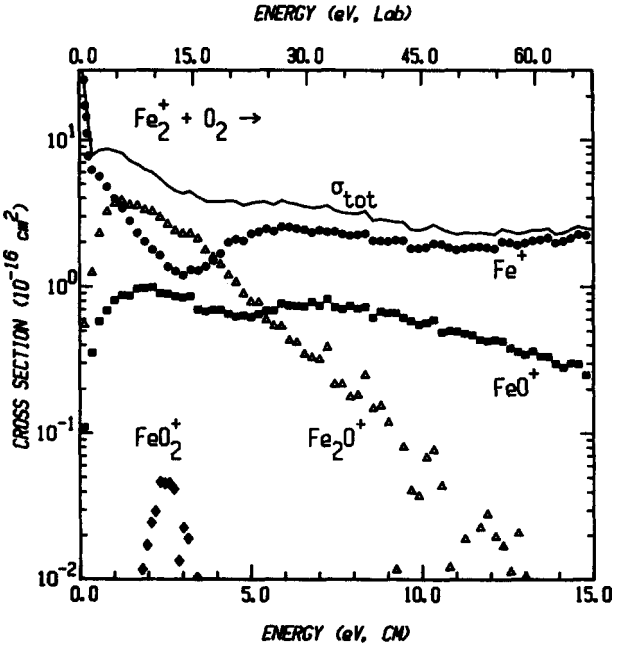

FIG. 2. The reaction of Fe_2^+ with O_2. The cross sections are plotted as functions of collision energy in the center-of-mass (lower x axis) and laboratory (upper x axis) frames.

TABLE II. $M_2^+ + O_2$ reaction pathways and thresholds.[a]

Reaction No.	Product channel	M = Fe (E_0)	M = Nb (E_0)
(6)	$M_2O^+ + O$	0.02 (0.05)[b,c]	<0[b,c]
(7)	$MO_2^+ + M$	0.7 (0.5)[c]	−1.4 (0.6)[c]
(8a)	$MO^+ + MO$	0.09 (0.14)[c]	−3.9 (0.3)[c]
(8b)	$MO^+ + M + O$	4.32 (0.09)[c]	4.2 (0.3)
(9a)	$M^+ + MO_2$	−0.9 (0.1)[c]	−3.53 (0.27)[c]
(9b)	$M^+ + M + O_2$	2.72 (0.07)[c]	6.15 (0.15)
(9c)	$M^+ + MO + O$	3.66 (0.12)	3.20 (0.27)[c]
(9d)	$M^+ + M + 2O$	7.89 (0.07)[c]	11.32 (0.15)

[a] In eV, uncertainties in parentheses. Calculated from data in Table I, except where noted.
[b] Derived in this study.
[c] The process is experimentally observed.

higher energies, σ_{tot} levels out to a nearly constant value of 2.5 Å^2, due to production of Fe^+ by dissociative processes. The magnitude of the cross section is close to the value expected for simple CID of Fe_2^+ by Xe,[34] in which $\sigma(Fe^+)$ was observed to reach a constant value of ~3 Å^2 at high energies.

A major reaction pathway for $Fe_2^+ + O_2$ is production of Fe_2O^+. This product is interesting because it requires the strong O_2 bond to be broken, while forming an oxide of the much more weakly bound iron dimer ion (Table I). How much Fe^+–Fe interaction remains in Fe_2O^+ is unknown, since these studies do not allow a definitive structural determination of the products. The cross section has a single feature, which is expected because reaction (6) is the only means of product formation (Table II). From a threshold of less than 0.1 eV, $\sigma(Fe_2O^+)$ rises, peaks at ~1.5 eV, and then falls off rapidly. Analysis using Eq. 3 with $N = 1.8$ and $E_0 = 0.02 \pm 0.05$ eV provides a good fit to the data. This model is shown in Fig. 3. Since $D^0(Fe_2^+\text{–O}) = D^0(O_2) - E_0$, the threshold gives $D^0(Fe_2^+\text{–O}) = 5.15 \pm 0.05$ eV.

FeO_2^+ is the least probable product ion of the four that are observed, having a maximum reaction cross section of ~0.05 Å^2. The only way that this product can be made is via reaction (7) (Table II) $Fe_2^+ + O_2 \rightarrow FeO_2^+ + Fe$. This process is in direct competition with $Fe_2^+ + O_2 \rightarrow Fe^+ + FeO_2$ [reaction (9a)]. From Fig. 2, it is evident that Fe^+ production is greatly favored over FeO_2^+ formation, in agreement with the relative I.P.s of FeO_2 and Fe in Table I. The threshold for reaction (7) is calculated from Table I to be 0.7 ± 0.5 eV (Table II). Unfortunately $\sigma(FeO_2^+)$ is too small to be analyzed definitively with Eq. (3). The apparent threshold of 1.6 ± 0.4 eV is only an upper limit to the true threshold because of the possibility of competition with other product channels and the small size of the cross section.

Production of the iron oxide ion FeO^+ is another possible pathway for the reaction of Fe_2^+ with O_2. Now the product ion can be formed via two reactions (8a) and (8b) (Table II). The low energy behavior of $\sigma(FeO^+)$ shows that this process is endothermic, although the apparent threshold is less than 0.1 eV. The cross section peaks at 2 eV then begins to decline. A higher energy process becomes apparent at 4–5 eV and then peaks near 7 eV. The low and high energy features in $\sigma(FeO^+)$ correspond well to reactions (8a) and (8b), respectively. At low energies, FeO^+ is produced exclusively by formation of $FeO^+ + FeO$. The onset of the high energy feature is consistent with the 4.3 ± 0.1 eV threshold calculated for formation of $FeO^+ + Fe + O$ [reaction (8b)].

The threshold for reaction (8a) is the sum of the bonds broken minus the sum of the bonds that are formed. Therefore, the following relationship holds, i.e.: $E_0(8a) = D^0(Fe_2^+) + D^0(O_2) - D^0(FeO) - D^0(Fe^+\text{–O})$. $E_0(8a)$ is calculated to be 0.09 ± 0.14 eV, using the values in Table I. The threshold region of the data is found to be best modeled by Eq. (3) using $N = 2.1$ and $E_0 = 0.01 \pm 0.05$ eV. This analysis, shown in Fig. 3, cannot fit the data at the lowest energies, which suggests that the cross section may have an exothermic component. However, since the reaction is so close to thermoneutral, this could be simply the result of reactions of Fe_2^+ and O_2 molecules with rotational energies (and possibly Fe_2^+ electronic energy) that are in the high energy tail of the thermal Boltzmann distribution ($kT = 0.026$ eV, 298 K).

Formation of Fe^+ dominates the reactivity at energies below about ~1.5 eV and at energies above ~4 eV, while at intermediate energies, Fe_2O^+ is the most intense product formed. Clearly, the "most probable process" depends on the energy of the reaction. As shown in Fig. 2, $\sigma(Fe^+)$ has several features. At the lowest energies, $\sigma(Fe^+)$ increases monotonically with decreasing energies as expected for an exothermic reaction. At ~3 eV, another product channel for Fe^+ formation turns on as evidenced by a sharp increase in the cross section. Another less dramatic rise in the cross

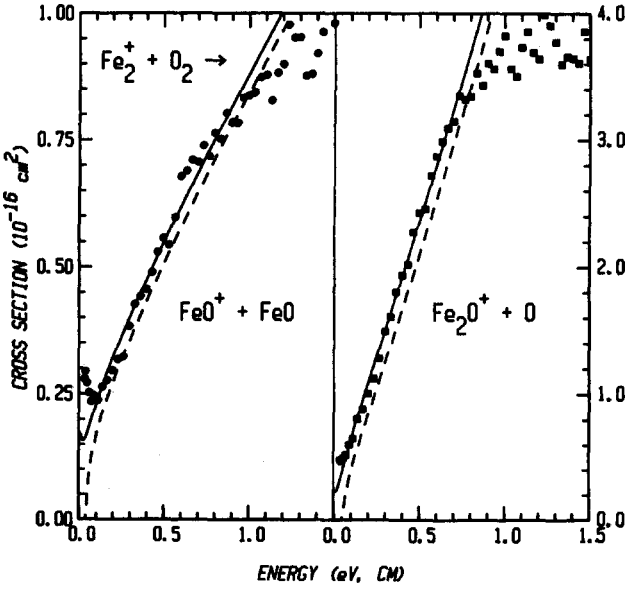

FIG. 3. Analyses of $Fe_2^+ + O_2 \rightarrow FeO^+ + FeO$ and $Fe_2^+ + O_2 \rightarrow Fe_2O^+ + O$ cross section thresholds. Note the different vertical scales for these two processes. The cross sections are plotted as functions of collision energy in the center-of-mass (lower x axis) frame. The experimental results (points) are compared with empirical models (dashed lines), discussed in the text, and their convolution with the experimental energy distributions (solid lines).

section is observed at ~9 eV. To find the origins of these features, we use the thermochemistry of all the possible reaction pathways that can produce Fe^+. The reactions [(9a)–(9d)] and their thresholds, calculated using the data in Table I, are provided in Table II. These thresholds can be associated with the onsets of the features observed in the Fe^+ cross section. Since reaction (9a) is the only exothermic process (Table II), formation of the $Fe^+ + FeO_2$ must take place at low energies. The CID process (9b) is readily apparent, since the cross section increases near $D^0(Fe_2^+) = 2.7$ eV. The rise in $\sigma(Fe^+)$ observed at energies ~9 eV is most probably due to reaction (9d). Formation of $Fe^+ + FeO + O$ [reaction (9c)] is not evident, possibly because it is hidden by the occurrence of reaction (9b).

3. $Fe_2^+ + O_2$: Reaction pathways

The products $FeO_2^+ + Fe$ and $Fe_2O^+ + O$ are formed in unique processes, such that there are no reaction pathways that can provide additional FeO_2^+ or Fe_2O^+ intensities at higher energies. On the other hand, these products can dissociate to a number of smaller products (Table III). This is also reflected in Table II which shows that there are several routes available for formation of smaller products at high energy. In this system, Fe^+ is particularly likely to be produced.

The Fe_2O^+ cross section, which is relatively large at low energies, shows a rapid falloff with increasing energy above ~4 eV. This is consistent with dissociation of Fe_2O^+ to $Fe^+ + FeO$ which becomes energetically accessible at 3.66 ± 0.12, or with fragmentation to $FeO^+ + Fe$ which can begin at 4.32 ± 0.09 eV. These dissociation pathways compete directly, since they differ only by the location of the charge. Formation of $FeO^+ + Fe$ is quite obvious as a second feature in $\sigma(FeO^+)$. $Fe^+ + FeO$ formation is not cleanly observed, since the threshold for this process appears to be obscured by the CID process that begins at 2.7 eV [reaction (9b)]. The Fe_2O^+ cross section is observed to peak at lower energies than ~3.7 eV, due to competition with the other product channels and possibly reaction dynamics.

Another possible way of forming FeO^+ is by dissociation of the FeO_2^+ product to $FeO^+ + O$. The small size of $\sigma(FeO_2^+)$ and the relatively large increase in $\sigma(FeO^+)$ indicates that FeO_2^+ fragmentation cannot be the main cause of the second feature in $\sigma(FeO^+)$. The second feature in $\sigma(FeO^+)$ must therefore be due to decomposition of Fe_2O^+. FeO_2^+ appears to dissociate to $Fe^+ + O_2$ via the overall process (9b), since $\sigma(FeO_2^+)$ begins to decline at 2.7 eV (Fig. 2). Above 8 eV, the FeO^+ cross section slowly declines with increasing energy, indicating that FeO^+ dissociates to Fe^+ and O [reaction (9d)]. This process, which can begin at 7.9 eV, is reflected in the Fe^+ channel, where a gradual but steady rise is noted with increasing energies.

4. $Fe_3^+ + O_2$: Thermochemistry and reaction products

With the addition of another Fe atom, the reactions become even more numerous and diverse. The energy dependence of the cross sections are shown in Fig. 4. All possible reactions are listed in Table IV. The thresholds are given where calculable from the data in Table I, or obtained from these experiments. The processes that appear as features in the cross sections are indicated in Table IV. Seven ionic products are possible, but only six are observed. FeO_2^+ is the only product ion that has a cross section below the experimental sensitivity of ~0.005 Å^2. Our failure to observe this product is reasonable, since we know that $I.P.(FeO_2) > I.P.(Fe) > I.P.(Fe_2)$ (Table I). Thus direct competition between the FeO_2^+ and Fe_2^+ products discriminates against FeO_2^+ production more severely than in the $Fe_2^+ + O_2$ system where FeO_2^+ was a minor product.

In the trimer system, the total cross section is smoothly varying. As shown in Fig. 5, σ_{tot} has the energy dependence predicted by the LGS model, although it has only half the predicted magnitude. Many of the individual product channels also exhibit this characteristic $E^{-1/2}$ behavior (Fig. 5). At these energies, the two most favorable ionic products are Fe_2O^+ and $Fe_2O_2^+$, the dimer ion oxides. Even at higher energies, Fe_2O^+ production remains a fairly important channel. At these energies, σ_{tot} decreases until it reaches a nearly constant value of 6 Å^2 (Fig. 4). The Fe_2^+ cross section clearly becomes dominant at these energies, but is smaller than the ~10 Å^2 magnitude observed in CID of Fe_3^+ by Xe. This difference is reasonable when the difference in molecular radii are considered. Based upon these consider-

TABLE III. $M_2^+ + O_2$ dissociation pathways and thresholds.[a]

Dissociation process	M = Fe (E_0)	M = Nb (E_0)	Reference reaction
$M_2O^+ + O \rightarrow M^+ + MO + O$	3.66 (0.12)	3.20 (0.27)[b]	(9c)
$M_2O^+ + O \rightarrow MO^+ + M + O$	4.32 (0.09)[b]	4.2 (0.3)	(8b)
$MO_2^+ + M \rightarrow MO^+ + O + M$	4.32 (0.09)	4.2 (0.3)[b]	(8b)
$MO_2^+ + M \rightarrow M^+ + O_2 + M$	2.72 (0.07)[b]	6.15 (0.15)	(9b)
$MO^+ + MO \rightarrow M^+ + O + MO$	3.66 (0.12)[b]	3.20 (0.27)	(8c)

[a] Thresholds (in eV) are for the overall reference reaction. Uncertainties are in parentheses. Calculated from data in Table I.
[b] The process is experimentally observed.

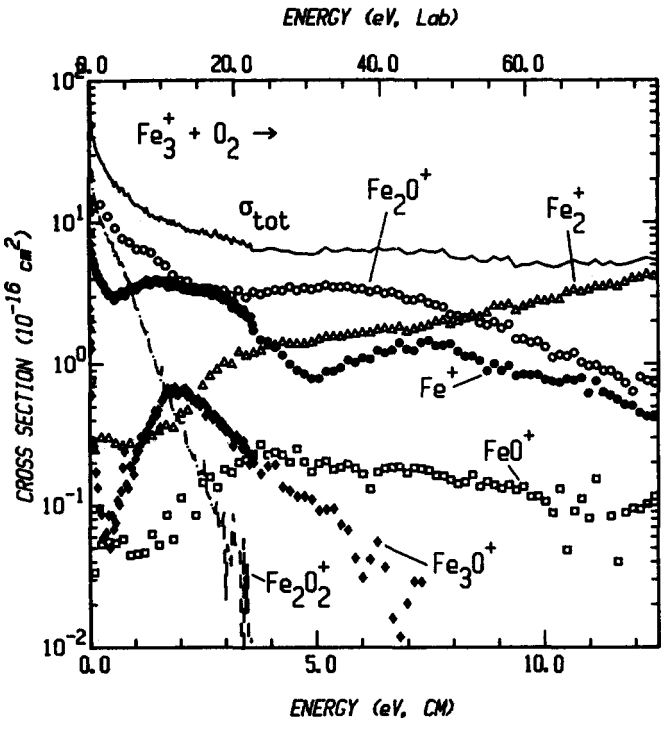

FIG. 4. The reaction of Fe_3^+ with O_2. The cross sections are plotted as functions of collision energy in the center-of-mass (lower x axis) and laboratory (upper x axis) frames.

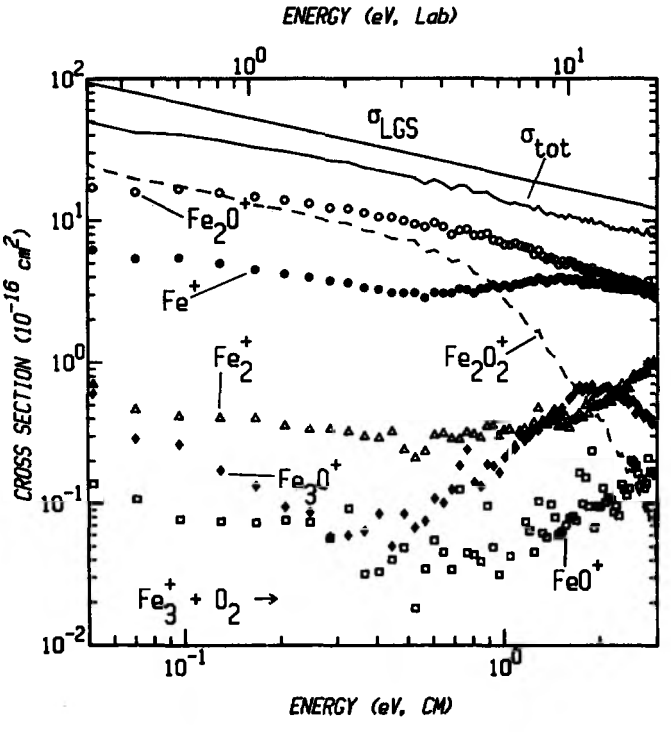

FIG. 5. Low energy behavior of the $Fe_3^+ + O_2$ reaction. The cross sections are plotted as functions of collision energy in the center-of-mass (lower x axis) and laboratory (upper x axis) frames. The Langevin–Gioumousis–Stevenson close collision cross section σ_{LGS} is shown as the straight line.

TABLE IV. $M_3^+ + O_2$ reaction pathways and thresholds.[a]

Reaction No.	Product channel	M = Fe (E_0)	M = Nb (E_0)
(10)	$M_3O^+ + O$	$<0^{b,g}$	$<0^{b,g}$
(11)	$M_2O_2^+ + M$	$<0^{b,g}$	$<0^{b,g}$
(12a)	$M_2O^+ + MO$	-2.57 (0.19)^{c,g}	<-3.75 (0.3)^{d,g}
(12b)	$M_2O^+ + M + O$	1.66 (0.16)^{c,g}	$\sim$4.4 (0.3)^{b,g}
(13a)	$M_2^+ + MO_2$	-1.96 (0.17)^{g}	-5.07 (0.27)^{g}
(13b)	$M_2^+ + M + O_2$	1.64 (0.15)^{g}	4.60 (0.15)
(13c)	$M_2^+ + MO + O$	2.58 (0.18)	1.65 (0.27)^{g}
(13d)	$M_2^+ + M + 2O$	6.81 (0.18)^{g}	9.77 (0.15)
(14a)	$MO_2^+ + M_2$	1.2 (0.7)	-2.0 (0.7)^{g}
(14b)	$MO_2^+ + M + M$	2.4 (0.7)	3.2 (0.6)
(15a)	$MO^+ + M_2O$	$<0^{b,g}$	$<0^{b,g}$
(15b)	$MO^+ + M_2 + O$	4.84 (0.18)	3.6 (0.4)
(15c)	$MO^+ + MO + M$	1.73 (0.19)^{g}	0.7 (0.4)^{g}
(15d)	$MO^+ + 2M + O$	5.96 (0.17)	8.8 (0.3)
(16a)	$M^+ + M_2O_2$	$<0^{h}$	$<0^{h}$
(16b)	$M^+ + M_2O + O$	<3.57 (0.06)^{e,h}	<7.0 (0.3)^{f,h}
(16c)	$M^+ + MO_2 + M$	0.8 (0.2)^{h}	1.08 (0.31)^{g}
(16d)	$M^+ + 2MO$	1.07 (0.22)^{g}	-0.32 (0.39)^{h}
(16e)	$M^+ + MO + M + O$	5.30 (0.19)	7.80 (0.31)
(16f)	$M^+ + M_2 + O_2$	3.24 (0.19)	5.56 (0.35)
(16g)	$M^+ + 2M + O_2$	4.36 (0.17)^{g}	10.75 (0.21)
(16h)	$M^+ + M_2 + 2O$	8.41 (0.19)	10.73 (0.35)
(16i)	$M^+ + 2M + 2O$	9.53 (0.17)	15.92 (0.21)

[a] In eV, uncertainties in parentheses. Calculated from data in Table I.
[b] Derived in this study.
[c] Calculated with $D^0(Fe_2^+–O) = 5.15 \pm 0.05$ eV.
[d] Calculated with $D^0(Nb_2^+–O) \approx 5.4 \pm 0.3$ eV.
[e] Calculated with $D^0(Fe_2–O) > 4.84 \pm 0.16$ eV and reaction (15a).
[f] Calculated with $D^0(Nb_2–O) > 3.7 \pm 0.3$ eV.
[g] The process is experimentally observed.
[h] The process may be observed, but is not uniquely identified.

ations, σ(CID) in the O_2 system should be $\sim 3/4\,\sigma$(CID) in the Xe system or ~ 7.5 Å^2. Thus it appears that simple CID may dominate at high energies.

The first reaction to be examined in this system is $Fe_3^+ + O_2 \rightarrow Fe_3O^+ + O$ [reaction (10) in Table IV]. At first glance $\sigma(Fe_3O^+)$ rises from a threshold of near 0.5 eV (Fig. 5), but the energy dependence below 0.4 eV indicates that $Fe_3O^+ + O$ production is exothermic. This in turn implies $D^0(Fe_3^+–O) > D^0(O_2) = 5.17$ eV. The cross section displays an unusual energy dependence. At energies less than 0.4 eV, the cross section declines with increasing energies more quickly than predicted by the LGS model. Above 0.4 eV, $\sigma(Fe_3O^+)$ increases and peaks at ~ 2 eV before declining quickly with increasing energies. This type of behavior is not easily explained since Fe_3O^+ can be formed by only one chemical reaction.

$Fe_2O_2^+$ is also formed by a single process [reaction (11)], but $\sigma(Fe_2O_2^+)$ displays a behavior that is more typical of an exothermic cross section. At the lowest energies, the cross section is very large rivaling that of Fe_2O^+, but decreases monotonically with increasing energies. $\sigma(Fe_2O_2^+)$ falls off much more quickly than predicted by the LGS model, starting at about 0.5 eV. Since this process is observed to be exothermic, we determine the limit $D^0(Fe_2^+–O_2) > D^0(Fe_2^+–Fe) = 1.64 \pm 0.15$ eV.

Fe_2O^+ is one of the most probable ionic products. The cross section is exothermic, as can be seen by its behavior at the lowest energies. Correspondingly, $Fe_2O^+ + FeO$ production [reaction (12a)] is calculated to be exothermic by 2.6 eV [using $D^0(Fe_2^+–O) = 5.15 \pm 0.05$ eV derived in the Fe_2^+ system above]. A purely exothermic cross section is not observed in Fig. 4, as a second component clearly contributes to $\sigma(Fe_2O^+)$ above ~ 2 eV. In agreement, reaction (12b), production of $Fe_2O^+ + Fe + O$, has a calculated threshold of 1.7 eV.

The major product observed at high energies is Fe_2^+, but it also has an exothermic component (Fig. 5). Exothermic formation of Fe_2^+ must be accompanied by FeO_2, since the other processes that produce Fe_2^+ are calculated to be endothermic (Table IV). The CID process $Fe_3^+ + O_2 \rightarrow Fe_2^+ + Fe + O_2$ [reaction (13b)] is observed as the rise in the cross section near $D^0(Fe_2^+–Fe) = 1.64 \pm 0.15$ eV. CID of Fe_3^+ with Xe was discussed in a recent paper on small iron cluster ion CID.[23] It was found that the Fe_2^+ product cross section peaks at about 4 eV, then slowly decreases. This behavior is not observed here, because of competition with other reactions and because reactions (13c) and (13d) can provide additional Fe_2^+ intensity at high energies (Table IV). These processes evidently become sufficiently favorable that the Fe_2^+ cross section becomes the largest at high energies.

FeO^+ is a relatively minor product, although it can be formed by four processes (Table IV). At first glance, the cross section appears to be endothermic, since it rises with increasing energies. However, closer examination of the cross section at the lowest energies (Fig. 5) finds that the cross section behavior is actually exothermic. Therefore, the strengths of the bonds formed are greater than those that are broken in reaction (15a), i.e., $D^0(Fe_2–O) + D^0(Fe^+–O) > D^0(Fe^+–Fe_2) + D^0(O_2)$. Using the data in Table I, $D^0(Fe_2–O) > 4.84 \pm 0.16$ eV. One reason for the unusual behavior of $\sigma(FeO^+)$ at low energies is that production of $FeO^+ + Fe_2O$ [reaction (15a)] must compete with reaction (12a), production of $Fe_2O^+ + FeO$. These channels differ by the location of the ionic charge, such that the competition between channels, which favors Fe_2O^+, implies that I.P.(Fe_2O) < I.P.(FeO).

Fe^+ is the smallest ionic product that can be formed. As shown in Fig. 4, the cross section for Fe^+ production is exothermic. However, the energy dependence is tortuous, due to the many product channels for Fe^+ formation [reactions (16a)–(16i), Table IV]. $\sigma(Fe^+)$ increases at 4.5 ± 0.2 eV, as determined from analysis with Eq. (3),[40] as expected for reaction (16g), which has a calculated threshold of 4.36 ± 0.17 eV. This implies that Fe^+ is produced by CID of Fe_3^+ to Fe^+ and two Fe atoms. The onset of another process is observed at $\sim 0.6 \pm 0.4$ eV, also from analysis of a secondary threshold. This indicates that reactions (16c), (16d), and maybe (16b) are occurring. The exothermic portion of the cross section must therefore be due to reaction (16a). The observation that $\sigma(Fe^+ + Fe_2O_2)$ is smaller than $\sigma(Fe_2O_2^+ + Fe)$ implies that I.P.(Fe_2O_2) < I.P.(Fe).

5. $Fe_3^+ + O_2$: Reaction pathways

The Fe_3O^+ cross section declines rapidly with increasing energy above 1.8 eV because of Fe_3O^+ fragmentation. By examining the thermochemistry of the various dissociation pathways in Table V, formation of $Fe_2O^+ + Fe$ is the lowest energy dissociation process. At 1.7 eV, the threshold for this process, the Fe_2O^+ cross section rises correspondingly. Decomposition of Fe_3O^+ may also occur to $Fe_2^+ + FeO$ above 2.6 eV. The onset of this process is not readily observed as $\sigma(Fe_2^+)$ is in the process of rising due to the CID process.

$\sigma(Fe_2O_2^+)$ demonstrates an even faster decline with increasing energies than Fe_3O^+ does. Since there is a single process for product formation, no larger ionic products can dissociate to add intensity to this product channel. Additionally, dissociation of $Fe_2O_2^+$ via several fragmentation pathways can begin at low energies (Table V). The lowest energy dissociation route is to $Fe^+ + FeO_2$, which can begin at 0.8 (Table V). This appears to be the dominant dissociation pathway, because the large increase in $\sigma(Fe^+)$ corresponds most closely to the size of the decrease noted in $\sigma(Fe_2O_2^+)$. Three other possible dissociation pathways become available near 1.7 eV: formation of $Fe_2O^+ + O$, $FeO^+ + FeO$, and $Fe_2^+ + O_2$. From the relative sizes of the cross sections, the former channel may be a major decomposition channel, but the latter two channels are clearly small (Fig. 4).

The size of $\sigma(Fe_2O^+)$ above ~ 5 eV makes Fe_2O^+ a prime source of smaller ions, since products like Fe_3O^+ and $Fe_2O_2^+$ have mostly decomposed at these energies. In the dimer system, Fe_2O^+ was observed to dissociate to Fe^+ and FeO^+. In the trimer system, Fe^+ and FeO^+ also are formed by fragmentation of Fe_2O^+ at relatively low energies (Table V). At higher energies, the second feature in $\sigma(Fe_2O^+)$ be-

TABLE V. $M_3^+ + O_2$ dissociation pathways and thresholds.[a]

Dissociation process	M = Fe (E_0)	M = Nb (E_0)	Reference reaction
$M_3O^+ + O \rightarrow M_2O^+ + M + O$	1.66 (0.16)[b]	~4.4[b]	(12b)
$M_3O^+ + O \rightarrow M_2^+ + MO + O$	2.58 (0.18)	1.65 (0.27)[b]	(13c)
$M_3O^+ + O \rightarrow MO^+ + M_2 + O$	4.88 (0.18)	3.6 (0.4)	(15b)
$M_3O^+ + O \rightarrow M^+ + M_2O + O$	<3.57 (0.06)	<7.0[c]	(16b)
$M_2O_2^+ + M \rightarrow M_2O^+ + O + M$	1.66 (0.16)	~4.4	(12b)
$M_2O_2^+ + M \rightarrow MO_2^+ + 2M$	2.4 (0.7)	<4.60 (0.15)	(14b)
$M_2O_2^+ + M \rightarrow MO^+ + MO + M$	1.73 (0.19)[b]	0.7 (0.4)[b]	(15c)
$M_2O_2^+ + M \rightarrow M^+ + MO_2 + M$	0.8 (0.2)[b]	1.08 (0.31)[c]	(16c)
$M_2O_2^+ + M \rightarrow M_2^+ + O_2 + M$	1.64 (0.15)[b]	4.60 (0.15)	(13b)
$M_2O^+ + MO \rightarrow M_2^+ + O + MO$	2.58 (0.18)[b]	1.65 (0.27)[c]	(13c)
$M_2O^+ + MO \rightarrow MO^+ + M + MO$	1.73 (0.19)	0.7 (0.4)[b]	(15c)
$M_2O^+ + MO \rightarrow M^+ + 2MO$	1.07 (0.22)	−0.32 (0.39)[c]	(16d)
$MO_2^+ + M_2 \rightarrow MO^+ + O + M_2$	4.84 (0.18)	3.6 (0.4)	(15b)
$MO_2^+ + M_2 \rightarrow M^+ + O_2 + M_2$	3.24 (0.19)	5.56 (0.35)	(16f)

[a] Thresholds (in eV) are for the overall reference reaction. Uncertainties in parentheses. Calculated from data in Table I.
[b] The process is experimentally observed.
[c] The process may be observed, but is not uniquely identified.

gins to decline near 5 eV, apparently due to dissociation to $Fe^+ + FeO$, which has a rising cross section. Note that this product arises from a sequential dissociation process $Fe_2O_2^+ + Fe \rightarrow Fe_2O^+ + O + Fe \rightarrow Fe^+ + FeO + O + Fe$. $\sigma(Fe^+)$ rises near this threshold (5.30 eV), but experiences a falloff at the highest energies, perhaps due to loss of its precursor or to inefficient product collection at these energies. Formation of FeO^+ from fragmentation of Fe_2O^+ is one reason why $\sigma(FeO^+)$ does not decline within this energy range.

B. Niobium oxidation reactions

1. $Nb^+ + O_2$

Figure 6 shows that the reaction of the atomic niobium ion with O_2 is a relatively simple process. Formation of NbO^+, given by reaction (5) with $M^+ = Nb^+$, is exothermic. At the lowest energies, $\sigma(NbO^+)$ is large, reaching 100 Å^2 (Fig. 6). As the collision energy increases, the cross section declines rapidly. Both the energy dependence and magnitude of $\sigma(NbO^+)$ are modelled exceptionally well by the LGS model up to 1 eV, indicating that NbO^+ is formed on every collision. Since NbO^+ formation is exothermic, $D^0(Nb^+\text{–}O) > D^0(O_2) = 5.17$ eV, which is in agreement with the literature bond energy 7.09 ± 0.23 eV (Table I) and with a value of 7.0 ± 0.3 eV from preliminary analysis of our results for the reactions of Nb_n^+ with CO.[41] Unlike the O_2 system, the high CO BDE (11.1 eV) makes NbO^+ formation endothermic in this case.

2. $Nb_2^+ + O_2$: Thermochemistry and reaction products

Four products are observed in this reaction. As observed in Fig. 7, all are produced exothermically, in marked contrast to the Fe_2^+ system. σ_{tot} reflects this behavior, mimicking $\sigma(NbO^+)$ at the lowest energies and $\sigma(Nb^+)$ at the highest energies. The "most probable process" is once again clearly energy dependent. At high energies, σ_{tot} levels out to ~7 Å^2, which is notably higher than the high energy magnitude of ~3 Å^2 observed in the $Nb_2^+ + Xe$ CID process.[24]

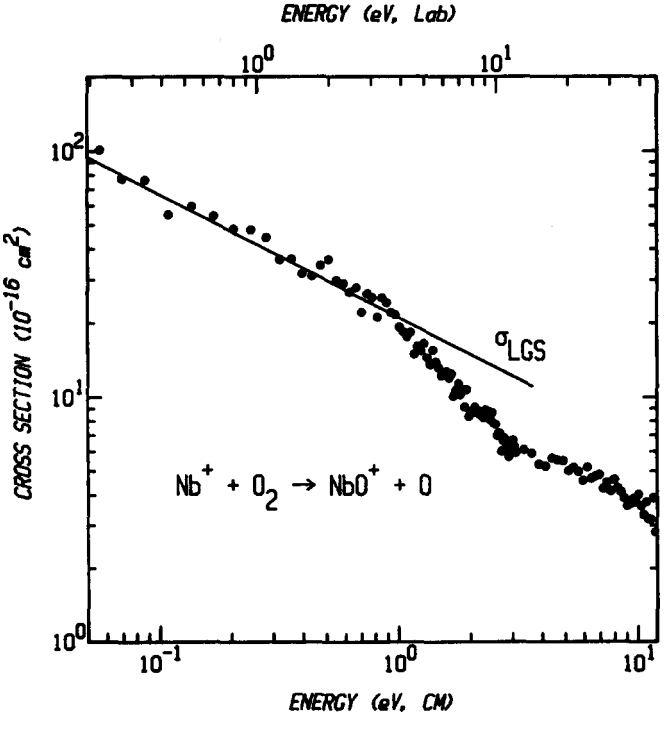

FIG. 6. Oxidation of the niobium atomic ion $Nb^+ + O_2 \rightarrow NbO^+ + O$. The cross section is plotted as a function of collision energy in the center-of-mass (lower x axis) and laboratory (upper x axis) frames. The Langevin–Gioumousis–Stevenson close collision cross section σ_{LGS} is shown as the straight line.

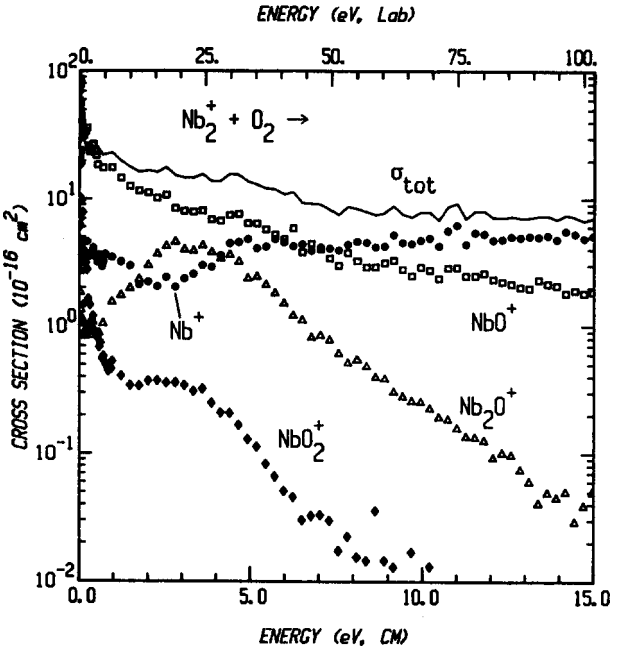

FIG. 7. The reaction of Nb_2^+ with O_2. The cross sections are plotted as functions of collision energy in the center-of-mass (lower x axis) and laboratory (upper x axis) frames.

This indicates that although Nb^+ may be produced by CID, it is also being formed by reactive processes. Comparison of σ_{tot} for the reactions of Nb_2^+ and Fe_2^+ with O_2 shows that Nb_2^+ is more reactive than Fe_2^+ by a factor of ~ 3.

$Nb_2O^+ + O$ is produced by reaction (6) (Table II). At the very lowest energies, $\sigma(Nb_2O^+)$ has an exothermic energy dependence from which we conclude that $D^0(Nb_2^+\text{–}O) > D^0(O_2) = 5.17$ eV. With increasing energies, the typical exothermic decline stops at 0.4 eV (Fig. 7) and the cross section rises to become the second most likely process from 2 to 4 eV. The cross section peaks at ~ 3 eV, then falls off rapidly. This complex type of behavior is similar to that observed in Fe_3O^+ formation. Like the production of Fe_3O^+, there is only one reaction that can form Nb_2O^+, which is in notable conflict with the more complicated cross section behavior.

Reaction (7), formation of the niobium dioxide ion, is the least probable process at most energies. From the low energy behavior of $\sigma(NbO_2^+)$, reaction (7) must be exothermic. Thus, $D^0(Nb^+\text{–}O_2) > D^0(Nb_2^+) = 6.15 \pm 0.15$ eV, consistent with the rough bond energy derived from literature data (Table I). While the dominance of $\sigma(Nb^+)$ over $\sigma(NbO_2^+)$ at most energies is consistent with the relative I.P.s in Table I, the production of $NbO_2^+ + Nb$ actually exceeds that of $Nb^+ + NbO_2$ below 0.2 eV (by a factor of 2 at 0.05 eV). This behavior cannot be explained by purely thermodynamic arguments, but must have a kinetic basis. Possible origins for this effect will be explored further below.

NbO^+ is the dominant product at lower energies and a major product throughout the energy range, as observed in Fig. 7. Formation of $NbO^+ + NbO$ is calculated to be exoergic by about 3.9 eV [reaction (8a), Table II). This is probably the main reason for the dominance of this product channel at low energies. Process (8b) is calculated to be endothermic by ~ 4.2 eV, but is not evident in the cross section. Instead, only a single exothermic feature is seen where $\sigma(NbO^+)$ decreases steadily with increasing energy.

Nb^+ can be formed by four separate reaction pathways given by reactions (9a)–(9d). As can be seen from Table II, reaction (9a) is the only exothermic reaction, so it must be responsible for the behavior of $\sigma(Nb^+)$ at the lowest energies. The CID process (9b) is not discernible here. Instead, $\sigma(Nb^+)$ increases sharply at the threshold for reaction (9c), in which NbO is formed. Reaction (9d) can contribute to $\sigma(Nb^+)$ only at the higher energies, but is not apparent.

3. $Nb_2^+ + O_2$: Reaction pathways

Rapid declines in the M_2O^+ and MO_2^+ cross sections (products that have only one pathway for formation) are again observed. Nb_2O^+ dissociates mainly to $Nb^+ + NbO$ at an energy threshold of 3.2 eV (Table III) as evidenced by the rapid decrease in $\sigma(Nb_2O^+)$ above 3 eV and by a corresponding rise in the Nb^+ cross section. Dissociation of Nb_2O^+ to $NbO^+ + Nb$ may occur starting at 4.2 eV, but is not obvious.

$\sigma(NbO_2^+)$ falls off more quickly than σ_{LGS} at the lowest energies. This is reasonable since $NbO_2^+ + Nb$ formation must compete with formation of $Nb^+ + NbO_2$, an energetically more favorable product channel. The decline in $\sigma(NbO_2^+)$ that begins at about 4 eV indicates that dissociation of NbO_2^+ to $NbO^+ + O$ occurs (Table III). NbO_2^+ can also fragment to $Nb^+ + O_2$ at 6.2 eV. Neither of these two processes are readily apparent in the daughter ion cross sections because of the small amount of NbO_2^+ product.

The $NbO^+ + NbO$ product channel can undergo dissociation to $Nb^+ + O + NbO$ [reaction (9c)] starting at 3.2 eV, although a rise is not readily observed in $\sigma(Nb^+)$. Complete atomization of the products requires at least 11.3 eV [reaction (9d), Table II]. Either reaction (9c) or reaction (9d) probably occurs at these higher energies, since $\sigma(Nb^+)$ continues to rise with increasing energy and $\sigma(NbO^+)$ continues to decline.

4. $Nb_3^+ + O_2$: Thermochemistry and reaction products

Reaction of the niobium trimer ion with O_2 forms all possible ionic products exothermically (Fig. 8). σ_{tot} decreases continually with increasing energy, as expected for exothermic reactions. In Fig. 9, the behavior exhibited below 1 eV is shown to be that of the LGS cross section within experimental uncertainties, indicating that Nb_3^+ reacts with O_2 on every collision. Above 1 eV, the cross section exceeds σ(LGS) as the interaction probability reaches a relatively constant value characteristic of a hard-sphere interaction. The most probable ionic products at low and high energies are Nb_2O^+ and Nb_2^+, respectively. Thus, the dominant product channels are qualitatively similar to those observed in the Fe_3^+ system. Here, at the highest energies, $\sigma(Nb^+)$ and $\sigma(Nb_2^+)$ are comparable to the cross sections observed in Nb_3^+ CID by Xe, suggesting that simple CID is a contributor to the high energy cross sections.

The first cross section that we examine in detail is

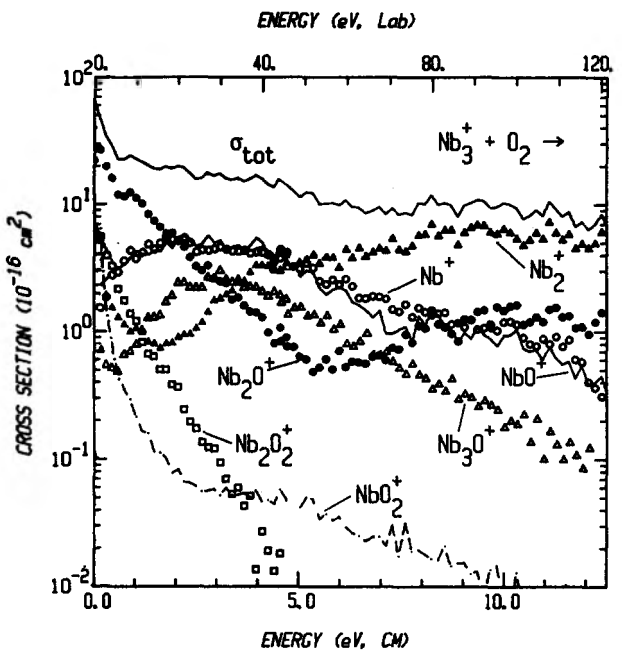

FIG. 8. The reaction of Nb_3^+ with O_2. The cross sections are plotted as functions of collision energy in the center-of-mass (lower x axis) and laboratory (upper x axis) frames.

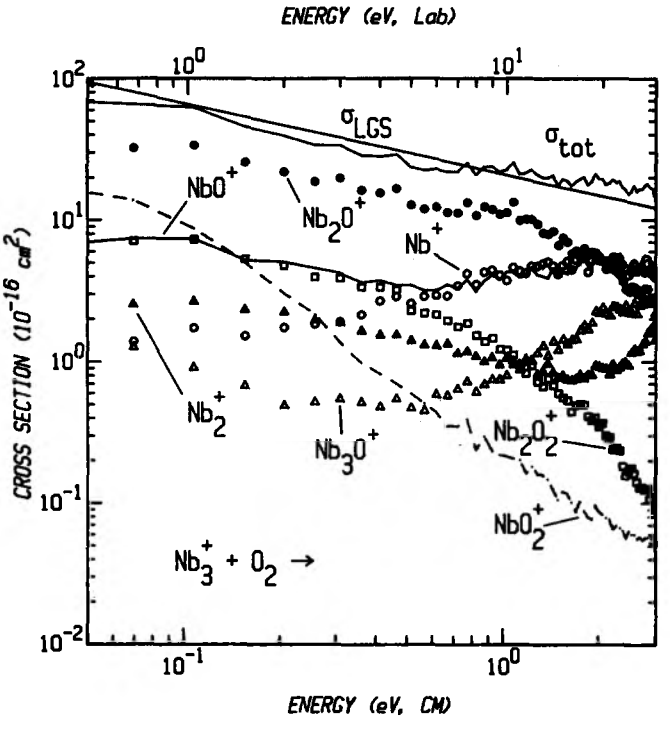

FIG. 9. Low energy behavior of the $Nb_3^+ + O_2$ reaction. The cross sections are plotted as functions of collision energy in the center-of-mass (lower x axis) and laboratory (upper x axis) frames. The Langevin–Gioumousis–Stevenson close collision cross section σ_{LGS} is shown as the straight line.

$\sigma(Nb_3O^+)$, where only reaction (10) of Table IV can form this product. At the lowest energies, the cross section behaves exothermically (Fig. 9). However, the cross section rises at energies above ~0.5 eV to peak at 2.5 eV and fall off with higher energies. In other words, $\sigma(Nb_3O^+)$ exhibits the same unusual behavior noted in formation of Fe_3O^+ and Nb_2O^+ in the systems above.

The cross section for $Nb_2O_2^+$ production [reaction (11)] declines percipitously such that $Nb_2O_2^+$ becomes the least favorable product by ~4 eV. As for $\sigma(Fe_2O_2^+)$, the observed decline is much sharper than the LGS model predicts at energies above ~0.6 eV. This is due primarily to decomposition and because the $Nb_2O_2^+$ product cannot be formed via decomposition of other ionic products. Note that below 0.5 eV, more $Nb_2O_2^+$ is formed than Nb^+ which is interesting because these products compete directly. While I.P.(Nb_2O_2) is unknown, it seems likely that it exceeds I.P.(Nb) based on the values of I.P.(NbO) and I.P.(NbO_2) (Table I). If true, the competition between $Nb_2O_2^+$ and Nb^+ is similar to that observed between NbO_2^+ and Nb^+ in the $Nb_2^+ + O_2$ system.

Formation of Nb_2O^+ is the major process observed at the lower energies. There are only two ways of forming Nb_2O^+, as shown in Table IV. Reaction (12b), the formation of $Nb_2O^+ + Nb + O$, has a threshold of $E_0 = D^0(Nb_2^+\text{–}Nb) + D^0(O_2) - D^0(Nb_2^+\text{–}O) = 9.8$ eV $- D^0(Nb_2^+\text{–}O)$. Since $D^0(Nb_2^+\text{–}O) > 5.17$ eV (derived in the Nb_2^+ system), the threshold for reaction (12b) is $< 4.6 \pm 0.15$ eV such that this process is probably endothermic. On the other hand, reaction (12a) (production of $Nb_2O^+ + NbO$), which has a threshold that is 8.1 eV lower than reaction (12b), is exothermic by at least 3.5 eV. To obtain a better estimate of $D^0(Nb_2^+\text{–}O)$, we analyze the higher energy feature in $\sigma(Nb_2O^+)$ to find a theshold of 4.4 ± 0.3 eV.[40] By attributing this feature to reaction (12b), this rough threshold gives $D^0(Nb_2^+\text{–}O) = 5.4 \pm 0.3$ eV, in agreement with the limit of > 5.17 eV. This value, although not rigorous due to the uncertainties of accounting for the exothermic Nb_2O^+ cross section, probably gives a reasonable estimate of $D^0(Nb_2^+\text{–}O)$. Therefore $D^0(Nb_2^+\text{–}O) < D^0(Nb^+\text{–}O)$ and reaction (12a) is exothermic by ~3.8 eV, consistent with the dominance of the Nb_2O^+ product at the lowest energies.

Nb_2^+ is the dominant ionic product at high energies. From its low energy behavior (Fig. 9), we can see that it is formed exothermically as predicted [reaction (13a), Table IV]. The rise in the cross section near 1.6 eV is due to reaction (13c) in which NbO + O are the neutral products. Nb_2^+ can also be formed by CID of Nb_3^+ beginning at 4.6 eV [reaction (13b)]. While no sharp increase in $\sigma(Nb_2^+)$ is noted at this energy, the cross section does rise slowly and steadily. Reaction (13d) may also take place at the higher energies via decomposition of larger product ions, contributing to make Nb_2^+ the most probable product at those energies.

The NbO_2^+ product can be formed via reactions (14a) and (14b). In contrast to the iron systems, a large quantity of this metal dioxide ion is produced, although only at the lowest energies indicating that at least reaction (14a) is occurring. The cross section declines much faster than σ_{LGS} with increasing energies (Fig. 9). Dissociation of NbO_2^+ to $NbO^+ + O$ or $Nb^+ + O_2$ can begin only at high energies (Table V). Thus, the rapid decline in $\sigma(NbO_2^+)$ at lower energies cannot be attributed to direct NbO_2^+ loss. Rather, the $NbO_2^+ + Nb_2$ products must compete with other prod-

uct channels such as $Nb_2^+ + NbO_2$ [reaction (13a)]. Note that $\sigma(NbO_2^+)$ exceeds $\sigma(Nb_2^+)$ at low energy, even though Table I indicates that I.P.(Nb_2) is about 3 eV lower than I.P.(NbO_2). This is qualitatively similar to the competion below NbO_2^+ and Nb^+ in the Nb_2^+ system, unusual behavior which is discussed further below.

At the lowest energies, $\sigma(NbO^+)$ increases with decreasing energies (Fig. 9), indicating an exothermic process. Since reactions (15b)–(15d) are calculated to be endothermic, this must be reaction (15a) suggesting that $D^0(Nb_2–O) > 3.6$ eV. The exothermic falloff in the cross section associated with reaction (15a) is interrupted near 0.7 eV, due to $NbO^+ + NbO + Nb$ formation [reaction (15c)]. Reactions (15b) and (15d) can contribute at higher energies, but are not clearly discernible as $\sigma(NbO^+)$ decreases with increasing energy above 3 eV.

Nb^+ can be formed in any of the nine different ways given in Table IV. $\sigma(Nb^+)$ shows a remarkably similar energy dependence to that of NbO^+, except at the very lowest energies. At higher energies, $\sigma(Nb^+)$, like $\sigma(NbO^+)$, does not exhibit sharp features which signal onsets of other routes to Nb^+ formation. Table IV shows that reactions (16a)–(16d) are the key reactions at low energies. Note that it is unlikely that reaction (16b) is exothermic since this would require that $D^0(Nb_2–O) > 10.7$ eV. Above about 1.1 ± 0.3 eV, reaction (16c) can occur and probably accounts for much of the rise in $\sigma(Nb^+)$. Table IV shows that reaction (16d) is probably exothermic, although within uncertainties, it could be endothermic by as much as 0.07 eV. In any case, reaction (16a) is more favorable energetically by the bond energy of Nb_2O_2 with respect to two NbO molecules. Thus, reaction (16a) will be exothermic in the likely event that $D^0(NbO–NbO) > 0.07$ eV. Despite the availability of these exothermic channels, $\sigma(Nb^+)$ increases monotonically with increasing energy at the lowest energies. This behavior is consistent with a barrier to formation of this product, although the barrier is small, certainly less than 0.1 eV. This unusual behavior of $\sigma(Nb^+)$ may be explained by the direct competition of reaction (16a) with reaction (11), formation of $Nb_2O_2^+ + Nb$. The latter channel is evidently favored at low energies, but then falls off quickly. As $\sigma(Nb_2O_2^+)$ declines, $Nb^+ + Nb_2O_2$ and $Nb^+ + 2\,NbO$ formation become more likely.

5. $Nb_3^+ + O_2$: Reaction pathways

$\sigma(Nb_3O^+)$ is interesting not only because it has the unusual energy dependence observed for the Nb_2O^+ and Fe_3O^+ cross sections in the systems examined above, but also because it declines much more gradually with increasing energies than observed in the iron cross sections. The slower decline in $\sigma(Nb_3O^+)$ observed in this system is probably attributable to the stability of the Nb_3O^+ product, i.e., the strengths of the Nb–O and Nb–Nb bonds. Nb_3O^+ dissociation can begin at ~ 1.7 eV to form $Nb_2^+ + NbO$ (Table V), but this process is not readily observed in $\sigma(Nb_3O^+)$. This cross section does decline at energies above 3–4 eV due to dissociation of Nb_3O^+ to either $NbO^+ + Nb_2$ or $Nb_2O^+ + Nb$ (Table V). The marked rise in Nb_2O^+ near 5 eV is a result of the latter process.

The cross section for $Nb_2O_2^+$ formation decays much more quickly with increasing energies than $\sigma(Nb_3O^+)$ does. This behavior is similar to the cross sections of other cluster dioxide ions in the systems discussed above. Fragmentation of $Nb_2O_2^+$ can begin at low energies, as shown in Table V, via formation of $NbO^+ + NbO$ ($E_0 = 0.7$ eV) and $Nb^+ + NbO_2$ ($E_0 = 1.1$ eV). $\sigma(Nb_2O_2^+)$ deviates from σ_{LGS} near 0.6 eV. This coincides with the increase in $\sigma(NbO^+)$ at 0.6 ± 0.4 eV, as determined from analysis,[40] which strongly suggests that $Nb_2O_2^+$ decomposes to $NbO^+ + NbO$. Decomposition to $Nb^+ + NbO_2$ is not observed as a distinct feature in $\sigma(Nb^+)$, which is rapidly changing at these energies. By ~ 4.6 eV, fragmentation of $Nb_2O_2^+$ to $Nb_2O^+ + O$, $NbO_2^+ + Nb$, and $Nb_2^+ + O_2$ can occur, but most of the $Nb_2O_2^+$ has already decomposed by this energy. This confirms that Nb_3O^+ is the major precursor to Nb_2O^+ at high energies.

At low energies, $\sigma(Nb_2O^+)$ parallels σ_{LGS}, even though dissociation of Nb_2O^+ to $Nb^+ + NbO$ is calculated to be exothermic (Table V). This process is most likely to be the dominant fragmentation route, at least until 0.7 eV, where formation of $NbO^+ + Nb$ can begin. Fragmentation to NbO^+ appears to occur, since there is a break in $\sigma(Nb_2O^+)$ at ~ 1 eV and, as previously noted, $\sigma(NbO^+)$ shows an increase at 0.6 ± 0.4 eV. Comparison of cross section magnitudes suggests that both $Nb_2O_2^+$ and Nb_2O^+ decompose to form Nb^+ and NbO^+. Nb_2O^+ may also decompose to Nb_2^+ at energies above 1.7 eV (Table V), contributing to the rise in $\sigma(Nb_2^+)$ seen at this energy.

Other sequential fragmentation processes are hard to unambiguously assign. $\sigma(NbO_2^+)$ falls off very quickly with increasing energies. NbO_2^+ should be fairly stable, since dissociation can only occur at energies above 3.6 eV to $NbO^+ + O$, or above 5.6 eV to $Nb^+ + O_2$ (Table V). The rapid decline of the cross section at lower energies therefore must be due to reaction competition, rather than NbO_2^+ fragmentation. The Nb_2^+ and NbO^+ products can dissociate to Nb^+. Neither fragmentation process is evident at these energies since $\sigma(Nb^+)$ and $\sigma(NbO^+)$ decrease smoothly and $\sigma(Nb_2^+)$ rises monotonically. Evidently fragmentation to the atomic ion is disfavored compared to reaction pathways which form the very strongly bound niobium oxides.

C. Comparison of reactivities

The iron and niobium cluster ion species examined here all show extensive reactivity toward O_2. Both metals react to form a plethora of products, mostly in exothermic processes. Both metals show the ability to form smaller bare ionic and neutral metal species as well as ionic and neutral metal monoxides and dioxides. Yet these metals also demonstrate distinct differences in reactivity.

1. Atomic ions

The atomic ions of iron and niobium represent the most strikingly different pair of reactants. FeO^+ formation is endothermic, while NbO^+ formation is exothermic. This dif-

ference is clearly noted in the behaviors of the cross sections (Figs. 1 and 6). The difference in reaction thermochemistry reflects the relative strengths of the NbO^+ and FeO^+ bonds (Table I). We may expect that the ability of niobium to form strong oxide bonds should dominate the reactivity of all Nb clusters, especially at low energies.

2. Dimer ions

The low energy portions of the dimer oxidation cross sections show this trend. In the Fe_2^+ system, all product channels, except $Fe^+ + FeO_2$, are endothermic (Fig. 2). In contrast, Nb_2^+ is highly reactive, forming all ionic products exothermically (Fig. 7). Of all these thermodynamically favorable reaction pathways, the dominant product channel is $NbO^+ + NbO$, formation of both the ionic and neutral monoxides. In the Fe_2^+ system, the similar product channel is much less favorable, being endothermic, although nearly thermoneutral. Further evidence of the influence of the stronger niobium–oxygen bonds is the observation that $\sigma(Nb_2O^+)$ peaks at a higher energy and declines much more slowly than $\sigma(Fe_2O^+)$.

At higher energies, the ionic products that are formed in the two dimer oxidation systems are qualitatively similar. The favored product is M^+. MO^+, M_2O^+, and MO_2^+ are observed with decreasing cross section magnitudes. However, the two systems go through different reaction pathways to form these products. For example, comparison to the CID results with Xe[24,34] shows that at high energies, Fe^+ is formed mainly by CID of Fe_2^+, while Nb^+ is accompanied by the NbO and O neutral products. $\sigma(MO^+)$ also shows differences at high energy. FeO^+ is observed to dissociate to $Fe^+ + O$ above ~ 7.9 eV, whereas NbO^+ is not observed to decompose to $Nb^+ + O$. These contrasting behaviors reflect the large differences in stabilities of MO^+ and MO for these two metals.

3. Trimer ions

Turning to the trimer systems, we see that Fe_3^+ reacts with O_2 to exothermically form all observed products (Figs. 4 and 5). Thus, Fe_3^+ is much more reactive toward O_2 than Fe_2^+ is, especially near thermal energies. This is probably because $D^0(Fe_2^+\text{–Fe}) < D^0(Fe_2^+)$ (Table I) such that product formation requires less energy for the trimer than for the dimer ion. This is also the case for the niobium trimer and dimer ions. Hence, it is not surprising that Nb_3^+ demonstrates somewhat higher reactivity than Nb_2^+.

In the Nb_3^+ system (Figs. 8 and 9), the dominant low energy product channels are the formation of metal monoxide products $Nb_2O^+ + NbO$ and $NbO^+ + Nb_2O$, even though these channels complete directly. The likelihood of metal monoxide production is consistent with formation of as many Nb–O bonds as possible. In the Fe_3^+ system, $Fe_2O^+ + FeO$ is the most probable channel, but $FeO^+ + Fe_2O$ is the least likely, presumably due to a larger difference in I.P.s.

In the $Fe_3^+ + O_2$ system, comparison of $\sigma(M^+)$ and $\sigma(M_2^+)$ to those observed from CID studies with Xe[23] shows that at high energy most bare metal ions are produced by CID. This is confirmed by the observation of distinct features with onsets that correspond to the direct CID processes. In the $Nb_3^+ + O_2$ system, the M^+ and M_2^+ cross sections at high energies are comparable to those observed in Xe CID studies,[24] but no distinct features corresponding to the CID thresholds can be seen. While direct CID is probably a contributor to $\sigma(Nb^+)$ and $\sigma(Nb_2^+)$ at high collision energies, reactive processes must be important sources of the bare niobium species at lower energies.

D. Unusual reaction dynamics: M_nO^+ and $M_nO_2^+$ products

1. $M_nO^+ + O$ reaction channel

The product channels which produce M_3O^+ from Fe_3^+ and Nb_3^+ and Nb_2O^+ from Nb_2^+ have energy dependences that are unusual for products which can only be formed by a single reaction. As described above, these cross sections exhibit exothermic behavior at the lowest energies, i.e., they decline as the energy is increased. However, in each case, the decline stops near 0.5 eV. The cross section then rises sharply, peaks, and resumes its decline. This second feature is larger than the first feature at their respective maxima in all cases. From preliminary studies of reactions of larger iron cluster ions with O_2, this behavior appears to be common for the $M_nO^+ + O$ product channel.

One possible influential factor in this behavior is conservation of angular momentum, which favors formation of products of equal masses. Simple angular momentum considerations[42] show that, e.g., formation of $Fe_3O^+ + O$ should be ~ 10 times less probable than $Fe_2^+ + FeO_2$ formation (assuming similar energetic requirements). So it is reasonable that $\sigma(Fe_3O^+)$ is much smaller than $\sigma(Fe_2^+)$ at the lowest energies. It is also reasonable from angular momentum considerations that the Fe_3O^+, Nb_3O^+, and Nb_2O^+ cross sections decrease faster than the LGS model predicts. Such behavior for exothermic reactions that form products with dissimilar masses is expected, based on angular momentum effects.[43] While these effects can help explain the relatively small size of the M_nO^+ product cross sections and their rapid decline, such reaction competition considerations cannot explain the two-component cross sections observed.

This cross section behavior implies that, in each system, two reactions take place—an exothermic reaction and an endothermic reaction. One way that a two-component cross section can be observed for a "single" process is if one reactant actually has two (or more) states available for reaction. Reactions of ground and excited states of atomic transition metal ions have been studied extensively in our laboratory.[44] In the systems studied here, the ground state presumably would be responsible for the endothermic process and the exothermic reaction would be attributed to a small population of electronically excited clusters. (While cluster vibrational excitation is also possible, this seems less plausible since the vibrational spacing is undoubtedly smaller than the ~ 0.5 eV spacing required to explain the observations here.) Reactant electronically excited states are an unlikely cause of the second cross section features, since these features become large at their maxima: $\sim 10\%$ of σ_{tot} for $Fe_3^+ + O_2$;

$\sim 25\%$ of σ_{tot} for $Nb_2^+ + O_2$; and $\sim 15\%$ of σ_{tot} for $Nb_3^+ + O_2$. This would require that an excited state (or states) is present in very high concentrations ($> 10\%$), or that it is orders of magnitude more reactive than the ground state.

Further, reactant excited states cannot explain the cross section behavior for two reasons. First, in our recent CID experiments on iron and niobium clusters,[23,24,34] we could find no evidence of such states. Nb and Fe dimers and trimers have clean dissociation thresholds, consistent with clusters that have little internal energy. In the only system that has been examined by other means, $D^0(Fe_2^+)$ derived from the CID threshold agrees with photodissociation results as well as the thermochemistry of reaction (8a) discussed below. The CID thresholds are also invariant with substantial changes in the source He stagnation pressure and the power of the vaporization laser. For these reasons, we concluded that our ions are at least thermalized, such that the proportion of excited state ions is small ($\leqslant 0.5\%$).

Second, production of $Nb_3O^+ + O$ should be a lower energy process than $Fe_3O^+ + O$ formation, since we have seen that Nb species generally form stronger bonds with oxygen than do Fe species. Instead we observe that the endothermic features in $\sigma(Fe_3O^+)$ and $\sigma(Nb_3O^+)$ have nearly identical thresholds (~ 0.5 eV). If this were due to discrete excited states of the trimer ions, then these states must have excitation energies that would cause nearly identical thresholds in these systems—an improbable coincidence. Thus, we find it unlikely that excited states of the *reactant* cluster ions are responsible for the observed two-component reactivities.

Another possible source of dual reactivities is formation of the ground state and an excited electronic state of the *products*. Such electronic states could be present in the form of M_3O^+ and Nb_2O^+ structural isomers. This may be plausible because isomers of bare niobium clusters have been postulated based on two-component reaction rates.[10,11] Excited product states (or isomers) would be consistent with our results if the ground-state products are formed with only a small probability at the thermodynamic limit; and if formation of an excited state of M_nO^+, a more probable process, occurs endothermically. The result would be a small exothermic cross section and a larger endothermic contribution at higher collision energies. If structural isomers are the cause of the observed behavior, cluster isomers may be much more pervasive than is currently believed. While this is a plausible explanation, it again implies an unusual coincidence. Namely, the various excited states (or isomers) just happen to have excitation energies such that the endothermic features all begin near 0.5 eV.

We believe that a likely cause for two-component cross section behaviors is a barrier in the entrance channel of this reaction. This argument considers that there are two mechanisms for formation of products from the ground-state reactants. In the dominant mechanism, facile production of $M_nO^+ + O$ involves formation of an intermediate, which requires a ~ 0.5 eV barrier to be surmounted. The second, but less probable way of M_nO^+ product formation involves an intermediate which can produce most other products at their thermodynamic limits, but cannot lead readily to $M_nO^+ + O$. Thus at low energies, exothermic M_nO^+ formation can only occur inefficiently, such that only small product intensities are observed. At energies near 0.5 eV, the higher energy intermediate becomes accessible, so that formation of M_nO^+ becomes allowed and readily observed. One possible reason that two such intermediates might compete is that formation of the energetically favorable intermediate is spin forbidden, while the higher energy intermediate can be formed in a spin-allowed process. Structural isomers of the intermediate might also explain such behavior.

As we have no way of probing the electronic states of the products or intermediates, both formation of excited electronic states (or isomers), or a barrier to formation of a suitable intermediate are distinct possibilities. We find this a very interesting problem that would benefit from theoretical investigation as well as further experimental studies.

2. Metal dioxide ion channels

The second unusual type of reaction observed in these systems is the surprising prevalence of metal dioxide ions at low energies. The cases of NbO_2^+ formation from the reaction of Nb_2^+ and Nb_3^+ are the clearest since the neutral products Nb and Nb_2, respectively, have *lower* ionization potentials than NbO_2 (Table I). Thus, the NbO_2^+ product is disfavored on thermodynamic grounds. The cases of $M_2O_2^+$ formation from reactions of Fe_3^+ and Nb_3^+ appear to also fall into this category, but are less clear cut since $IP(M_2O_2)$ are unknown.

In both systems, the NbO_2^+ cross sections decrease very rapidly with increasing energies and become very unlikely products at energies above a few eV. In contrast, the bare metal ion (atom or dimer) is formed in increasing yields with increasing energy, such that the thermodynamically favored bare metal ion species is favored above about 0.5 eV in both systems. The explanation for this may parallel that for the $M_n^+ + O_2 \rightarrow M_nO^+ + O$ reactions. Specifically, we can imagine that at low kinetic energies, a kinetically favored intermediate dissociates to yield NbO_2 with a different geometry than the ground state, thereby having a lower IP. Consequently, $NbO_2^+ + Nb_{n-1}$ is formed preferentially. As the energy is increased, the barrier to a more thermodynamically favored intermediate is overcome. This intermediate now dissociates to form ground-state NbO_2 with a high IP, such that $Nb_{n-1}^+ + NbO_2$ is preferentially formed. A speculative possibility is formation of Nb_n–O–$O^{\bullet +}$, which dissociates to form Nb_{n-1} + Nb–O–$O^{\bullet +}$. A more stable intermediate would have inserted into the O_2 bond and would then form an O–Nb–O structure.

E. Thermochemical data

The BDE and IP values for the niobium and iron oxide species determined here are summarized in Table VI. Quantitative Fe_2^+–O and Fe^+–O BDEs are determined in this study and limits on most other BDEs are set by observation of exothermic reactions. Since no specific values are obtained for the niobium oxides BDEs, only the iron systems deserve further discussion.

The threshold for $Fe_2^+ + O_2 \rightarrow FeO^+ + FeO$ [reaction

TABLE VI. Bond energies (at 298 K) derived in this study.[a]

Bond	M = Fe	M = Nb
M_2^+–O	5.15 (0.05)	~5.4 (0.3), >5.17
M_2–O	>4.84 (0.16)	>3.7 (0.5)
M_2^+–O_2	>1.64 (0.15)	>4.60 (0.15)
M_3^+–O	>5.17 (0.001)	>5.17 (0.001)

[a] Values in eV, uncertainties in parentheses.

(8a)] is shown in Fig. 3. In our experiments, Fe_2^+ and O_2 are presumed to have thermal energy distributions as are the products, so that $E_0(298\ \text{K}) = D^0_{298}(Fe_2^+) + D^0_{298}(O_2) - D^0_{298}(FeO) - D^0_{298}(Fe^+\text{–O})$. Using values from Table I, this means that $D^0(FeO) + D^0(Fe^+\text{–O}) = 2.72 (\pm 0.07) \pm 5.17(\pm 0.001) - 0.01 \pm 0.05 = 7.88 \pm 0.09$ eV. Using our previously determined value of $D^0_{298}(Fe^+\text{–O}) = 3.57 \pm 0.06$ eV,[36] we find that $D^0_{298}(FeO) = 4.31 \pm 0.10$ eV. This is in reasonable agreement with the literature value $D^0(FeO) = 4.23 \pm 0.10$ eV (Table I). The threshold also allows an independent determination of IP (FeO) with the relation $IP(FeO) = IP(Fe) + D^0(FeO) - D^0(Fe^+\text{–O})$. Using our value for $D^0(FeO) = 4.31$ eV and $D^0(Fe^+\text{–O})$, we find $IP(FeO) - IP(Fe) = 0.74 \pm 0.12$ eV, or $IP(FeO) = 8.64 \pm 0.12$ eV. This is also in reasonable agreement with the literature value of 8.71 ± 0.10 eV.[45]

In the $Fe_2^+ + O_2 \rightarrow FeO^+ + FeO$ reaction, an activation barrier could conceivably be present, if, for instance, the reaction were to involve a tight four-center transition state. Comparison of the experimental threshold (0.01 ± 0.05 eV) and the threshold calculated from Table I (0.09 ± 0.14 eV) means that an activation barrier is not present. Moreover, the agreement indicates that the Fe_2^+, FeO^+, and FeO BDEs are mutually consistent within their experimental uncertainties. This helps confirm the accuracy of the results presented here, and indicates that the Fe_2^+ ions are thermalized.

$D^0(Fe_2^+\text{–O})$ is also determined from this study to be 5.15 ± 0.05 eV. By examining Table VI, the relative binding energies of an oxygen atom to various bare iron species can be compared. We find that $D^0(Fe^+\text{–O}) < D^0(Fe_2^+\text{–O}) < D^0(Fe_3^+\text{–O})$ and that $D^0(Fe\text{–O}) < D^0(Fe_2\text{–O})$. The oxygen binding energy increases as the number of Fe atoms increases for both the ions and the neutrals. One way that this observation can be rationalized is if the O atom is bound to more than one Fe atom. Such a situation could be facilitated by incorporating the O atom into the cluster either by insertion, or by placing the O atom in a bridging site, rather than an axial position.

F. Implications for flow tube experiments

As pointed out in the opening remarks, most studies of cluster reactivities have been done on neutral clusters with flow tube techniques. These reactions take place at thermal energies, such that only exothermic or thermoneutral reactions can be observed. Additionally, reactions take place directly after cluster formation, such that only mass *distributions* with and without reactant are known. The exact identities of the parent reactants are not unambiguously connected with the observed products. Thus many of the details of the reactions cannot be determined unequivocally.

The reactions studied in this work underline the possibility of fragmentation reactions of cluster ions and neutrals in flow tube experiments. Although cluster ions are probably formed in small numbers with respect to the neutral clusters, they may be somewhat more reactive because of the attractive ion-induced dipole potential. Also we may expect that reactions of neutral clusters have products that are similar to those observed here for the ionic clusters. In this study, the reactions of the dimer and trimer ions with oxygen are observed to form smaller bare ionic and neutral clusters [see, for instance, reaction (13a), Table IV]. We have also observed products of this type in preliminary oxidation studies of larger Nb_n^+ and Fe_n^+ clusters. In flow tube studies, these fragmentation products of neutral and ion clusters can react further, either by subsequent fragmentation, or by more extensive oxidation. This makes identification of the reaction difficult. Furthermore, detection of bare metal products may cause misleading conclusions, because these species cannot be distinguished from smaller clusters that do not react.

In the systems studied here, it is apparent that all of these species, with the exception of Fe^+, undergo extensive oxidation, forming ionic and neutral oxides exothermically. As has been noted previously, some clusters can have reactivities that are activated or deactivated by an additional oxygen atom.[28] Therefore, flow tube product distributions may also be affected by the presence of neutral and ionic metal cluster oxides that are initially formed in cluster sources. The reactivity of the oxides themselves are an interesting area which we hope to address in the future.

V. CONCLUSIONS

These systems demonstrate the diverse and complex reactivities that transition metal cluster ions can have and that the use of ion beam techniques allows investigation and an understanding of the reactivities of metal clusters. Quantitative reaction thermochemistry can be obtained from endothermic reactions which have distinct energy thresholds. Limits can be set from the observation of reactions that are exothermic. The kinetic information that is furnished by this study, in combination with the bond dissociation energies, yields a fairly comprehensive picture of the oxidation of these clusters. Since more information can be obtained from endothermic reactions, measurements of the reactivity of these clusters toward CO are already underway. These reactions are endothermic because of the strong bond CO bond of 11.1 eV. Such studies will provide further delineation of niobium and iron oxide BDEs and IPs.

Extending these studies to larger clusters of these same metals may help to answer several questions. Do changes in reactivity occur gradually or suddenly at a specific cluster size? Do these changes occur at large or small cluster sizes? Such qualitative information on larger clusters can certainly be obtained from ion beam studies. Although the number of reaction pathways grows geometrically with cluster size,

quantitative information may still be extracted with careful analysis of the cross sections in combination with information gained from studies of the smaller cluster building blocks. Another tactic that can be used to gain a more universal understanding of cluster chemistry is to conduct similar studies of other transition metal cluster ions. From these investigations, we hope to understand the characteristic differences and similarities in reactivities of these metals.

ACKNOWLEDGMENT

This work was supported by the Army Research Office, DAAL03-87-2211.

[1]T. G. Dietz, M. A. Duncan, D. E. Powers, and R. E. Smalley, J. Chem. Phys. **74**, 6511 (1981); V. E. Bondybey and J. H. English, *ibid.* **76**, 2165 (1982).

[2](a) D. M. Cox, R. L. Whetten, M. R. Zakin, D. J. Trevor, K. C. Reichmann, and A. Kaldor, Proc. Int. Laser Sci. Conf. **146**, 527 (1986); (b) E. A. Rohlfing, D. M. Cox, and A. Kaldor, J. Phys. Chem. **88**, 4497 (1984); (c) D. E. Powers, S. G. Hansen, M. E. Geusic, D. L. Michalopoulos, and R. E. Smalley, J. Chem. Phys. **78**, 2866 (1983); (d) E. A. Rohlfing, D. M. Cox, A. Kaldor, and K. H. Johnson, *ibid.* **81**, 3846 (1984).

[3]Spectroscopic work on dimers has recently been reviewed in M. D. Morse, Chem. Rev. **86**, 1049 (1986).

[4]Work on metal trimers is just beginning; see Z. Fu, G. W. Lemire, Y. M. Hamrick, S. Taylor, J.-C. Shiu, and M. D. Morse, J. Chem. Phys. **88**, 3524 (1988).

[5]D. M. Cox, D. J. Trevor, R. L. Whetten, E. A. Rohlfing, and A. Kaldor, Phys. Rev. B **32**, 7290 (1985).

[6]E. K. Parks, B. H. Weiller, P. S. Bechthold, W. F. Hoffman, G. C. Nieman, L. G. Pobo, and S. J. Riley, J. Chem. Phys. **88**, 1622 (1988); E. K. Parks, G. C. Nieman, L. G. Pobo, and S. J. Riley, *ibid.* **88**, 6260 (1988).

[7]M. D. Morse, M. E. Geusic, J. R. Heath, and R. E. Smalley, J. Chem. Phys. **83**, 2293 (1985).

[8]R. L. Whetten, D. M. Cox, D. J. Trevor, and A. Kaldor, J. Phys. Chem. **89**, 566 (1985).

[9]M. E. Geusic, M. D. Morse, and R. E. Smalley, J. Chem. Phys. **82**, 590 (1985).

[10]Y. Hamrick, S. Taylor, G. W. Lemire, Z.-W. Fu, J.-C. Shui, and M. D. Morse, J. Chem. Phys. **88**, 4095 (1988).

[11]M. R. Zakin, R. O. Brickman, D. M. Cox, and A. Kaldor, J. Chem. Phys. **88**, 3555 (1988).

[12]M. R. Zakin, D. M. Cox, and A. Kaldor, J. Phys. Chem. **91**, 5224 (1987).

[13]R. J. St. Pierre and M. A. El-Sayed, J. Phys. Chem. **91**, 763 (1987).

[14]R. J. St. Pierre, E. L. Chronister, and M. A. El-Sayed, J. Phys. Chem. **91**, 5228 (1987).

[15]S. J. Riley, E. K. Parks, G. C. Nieman, L. G. Pobo, and S. Wexler, J. Chem. Phys. **80**, 1360 (1984); G. C. Nieman, E. K. Parks, S. C. Richtsmeier, K. Liu, L. G. Pobo, and S. J. Riley, High Temp. Sci. **22**, 115 (1986).

[16]K. Ervin, S. K. Loh, N. Aristov, and P. B. Armentrout, J. Phys. Chem. **87**, 3593 (1983).

[17]P. B. Armentrout, S. K. Loh, and K. Ervin, J. Am. Chem. Soc. **106**, 1161 (1984). Mn_2^+ was found to be unreactive with alkanes in ICR studies [R. B. Freas and D. P. Ridge, J. Am. Chem. Soc. **102**, 7129 (1980)].

[18](a) M. F. Jarrold and J. E. Bower, J. Chem. Phys. **85**, 5373 (1986); (b) **87**, 5728 (1987).

[19]S. A. Ruatta and S. L. Anderson, J. Chem. Phys. **89**, 273 (1988).

[20]M. F. Jarrold and J. E. Bower, J. Am. Chem. Soc. **110**, 70 (1988).

[21]See, e.g., L. Hanley and S. L. Anderson, J. Phys. Chem. **91**, 5161 (1987) and M. F. Jarrold and J. E. Bower, J. Chem. Phys. **87**, 1610 (1987).

[22]P. J. Brucat, L.-S. Zheng, C. L. Pettiette, S. Yang, and R. E. Smalley, J. Chem. Phys. **84**, 3078 (1986).

[23]S. K. Loh, D. A. Hales, L. Lian, and P. B. Armentrout, J. Chem. Phys. **90**, 5466 (1989).

[24]S. K. Loh, L. Lian, and P. B. Armentrout, J. Am. Chem. Soc. **111**, 3167 (1989).

[25]D. B. Jacobson and B. S. Freiser, J. Am. Chem. Soc. **106**, 4623 (1984).

[26]D. B. Jacobson and B. S. Freiser, J. Am. Chem. Soc. **107**, 1581 (1985).

[27]J. M. Alford, P. E. Williams, D. J. Trevor, and R. E. Smalley, Int. J. Mass Spectrom. Ion Processes **72**, 33 (1986).

[28]J. M. Alford, F. D. Weiss, R. T. Laaksonen, and R. E. Smalley, J. Phys. Chem. **90**, 4480 (1986).

[29]M. R. Zakin, R. O. Brickman, D. M. Cox, and A. Kaldor, J. Chem. Phys. **88**, 6605 (1988).

[30]S. K. Loh, D. A. Hales, and P. B. Armentrout, Chem. Phys. Lett. **129**, 527 (1986).

[31]R. Campargue, J. Phys. Chem. **88**, 4466 (1984); J. P. Toennies and K. Winkelmann, J. Chem. Phys. **66**, 3965 (1977).

[32]K. M. Ervin and P. B. Armentrout, J. Chem. Phys. **83**, 166 (1985).

[33]There is a 5% probability of a single collision for a collision cross section of 20 $Å^2$.

[34]S. K. Loh, L. Lian, D. A. Hales, and P. B. Armentrout, J. Phys. Chem. **92**, 4009 (1988).

[35](a) L. Sunderlin, N. Aristov, and P. B. Armentrout, J. Am. Chem. Soc. **109**, 78 (1987); (b) N. Aristov and P. B. Armentrout, *ibid.* **108**, 1806 (1986); (c) B. H. Boo and P. B. Armentrout, *ibid.* **109**, 3549 (1987); (d) J. L. Elkind and P. B. Armentrout, J. Phys. Chem. **91**, 2037 (1987).

[36]S. K. Loh, E. R. Fisher, L. Lian, R. H. Schultz, and P. B. Armentrout, J. Phys. Chem. **93**, 3159 (1989).

[37]I. Shim and K. A. Gingerich, J. Chem. Phys. **77**, 2490 (1982).

[38]S. P. Walch and C. W. Bauschlicher, in *Comparison of Ab Initio Quantum Chemistry with Experiment*, edited by R. J. Bartlett (Reidel, Dordrecht, 1985).

[39]G. Gioumousis and D. P. Stevenson, J. Chem. Phys. **29**, 292 (1958).

[40]Analysis of secondary features is accomplished by first removing the primary lower energy feature by subtracting a semilogarithmic fit of the low energy cross section behavior. The second feature is then fit using Eq. (3), as described for primary features.

[41]L. Lian, S. K. Loh, and P. B. Armentrout (in progress).

[42]Conservation of momentum requires that $L = \mu v b = L' = \mu' v' b'$, where μ is the reduced mass, b is the impact parameter, and v is the relative particle velocity. The prime indicates post reaction conditions. Also, the rotational angular momenta J and J' are generally considered to be small compared to L and L'. When μ' is much less than μ (as is the case for products of disproportionate masses), it becomes more difficult to conserve angular momentum, i.e., either v' or b' must be much larger than v or b to compensate. Since v' depends on the energetics of the reaction, the result can be a limit on the available values of b' and thus on the reaction cross section (since $\sigma \propto b'^2$). Details of these ideas are contained in Refs. 35(a) and 43.

[43]J. D. Burley, K. M. Ervin, and P. B. Armentrout, Int. J. Mass. Spectrom. Ion Processes **80**, 153 (1987).

[44]P. B. Armentrout, in *Structure/Reactivity and Thermochemistry of Ions*, edited by P. Ausloos and S. G. Lias (Reidel, Dordrecht, 1987), pp. 97–164.

[45]D. L. Hildenbrand, Chem. Phys. Lett. **34**, 352 (1975).